

Magneto-responsive particle targeting and deposition in the presence of an external magnetic field for cardiovascular stenting therapy

Doctoral Thesis - Abstract

for obtaining the scientific title of doctor at

Politehnica University Timișoara

in the field of *Mechanical Engineering*

author eng. Maria-Cristina Ioncica (married Macovei)

PhD coordinator Scientific researcher I, dr. eng. Șandor Ianos Bernad

month 07 year 2024

The PhD thesis investigates experimental and numerical aspects of the magnetic drug targeting process (MDT) using an external magnetic field generated by permanent magnets. MDT is a non-invasive method that involves the use of an external magnetic field to target drug-loaded magnetic particles to specific locations within the body [1]. The paper is divided into 11 chapters, each dealing individually with a different issue. The chapters of the PhD thesis are the following: 1. Introduction, 2. Materials and methods for the experimental investigation of the targeting process, 3. Magnetic nanoparticles for the drug targeting process, 4. Synthesis and characterization of surface functionalized magnetic nanoparticles, 5. Synthesis and characterization of surface functionalized magnetic clusters, 6. Investigation and analysis of the magnetic field generated by permanent magnets, 7. Numerical simulation of two-phase flow in specific geometries for drug targeting applications, 8. Experimental investigation of controlled targeting and deposition of magnetic particles in a straight artery model, 9. Experimental investigation of controlled targeting and deposition of magnetic particles in a stented artery model, 10. General conclusions of the PhD thesis, and 11. Personal contributions and perspectives.

Chapter 1, entitled "**Introduction**", deals with the general concepts of different types of cardiovascular diseases, the use of the targeting process for them, and the advantages and disadvantages associated with the process. Figure 1 shows the mode of action of the magnetic drug targeting process inside a blood vessel.

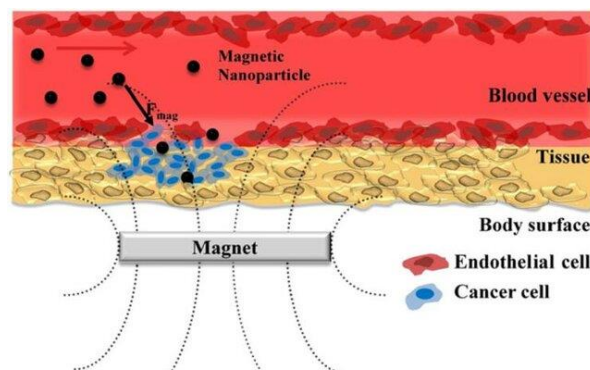


Figure 1. Representation of the magnetic drug targeting process (MDT). Figure modified according to [2].

The choice of cardiovascular diseases field is due to its global incidence. According to the World Heart Federation (WHF), cardiovascular diseases are one of the leading causes of death globally, and the number is expected to rise due to the increased risk of triggering factors (smoking, obesity, diabetes, etc.) [3]. Although according to scientific studies [4–9] it has been shown that the MDT process may have applications in several types of cardiovascular diseases, for the present PhD thesis the research is focused on atherosclerosis and its associated stented area. Atherosclerosis can be defined as an accumulation of fats, cholesterol and other substances inside the artery and on the arterial walls, which can lead to blockages of the artery, preventing blood flow, or to ruptures, favoring the development of thrombi [10]. One of the treatment methods for atherosclerosis is the stenting procedure, which involves inserting a metallic or polymeric mesh tube into the blood vessel using a thin catheter and a balloon, followed by the inflation of the balloon and, consequently, expansion of the stent. This process is used as to restore normal blood flow in the narrowed or blocked artery. Figure 2 shows the stenting procedure in a narrowed artery.

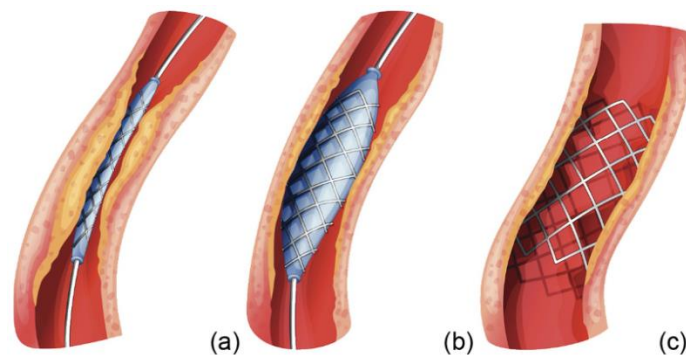


Figure 2. Stenting procedure: a) introduction and positioning of the stent in the desired region of the artery; b) balloon inflation and stent expansion; and c) unobstructed artery. Modified according to [11].

The use of stents to restore blood flow can lead to arterial wall damage, requiring drug treatment. In order to minimize the side effects of the systemic administration of the medication, an alternative is the use of the MDT process. Some of the advantages of this process are: it is non-invasive and allows magnetic particles to be targeted to specific tissues or areas in the body by an external magnetic field, it increases the concentration of the medication in the specific area leading to prolonged drug retention, and it reduces the exposure of healthy tissues to harmful concentrations of medication, with potential side effects on normal cells being minimized [12].

This thesis deals with issues ranging from the synthesis of magnetic particles/clusters for medical applications to experimental investigations related to the targeting process in two different types of arterial models. The thesis intends to provide a clear insight into the concepts and investigations required for the targeting process, as well as the drawbacks and impediments that may arise. The thesis provides qualitative results regarding different types of nanoparticles and magnetic clusters and their potential applicability for the biomedical field.

Chapter 2, entitled "**Materials and methods for experimental investigation of the targeting process**", discusses the equipment and materials used for the magnetic particle targeting process in two different types of arterial models (straight artery and stented artery). The outline of the experimental stand is shown in Figure 3.

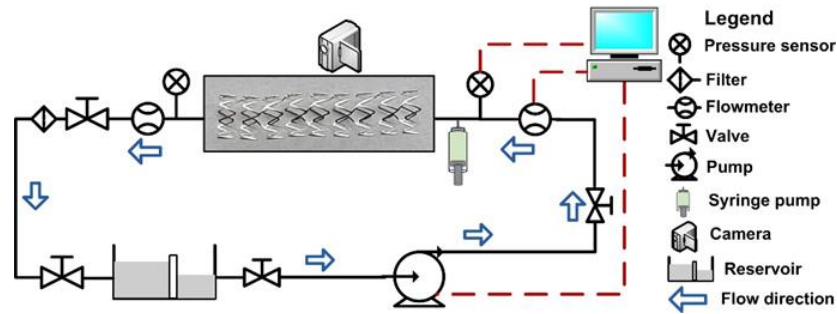


Figure 3. Experimental setup and its components used for the magnetic targeting process in a stented artery model.

For the experimental investigation of the targeting process for the stented artery, a ferromagnetic metallic stent, i.e. a stent that exhibits magnetization, was used. The advantage of using this type of stent is that it behaves like a magnet under the action of an external magnetic field and has the property of attracting magnetic particles/clusters. The fluids used for the targeting process were as follows:

- A blood analogous fluid, consisting of a water – glycerol mixture and with a density close to that of the blood ($\rho = 1055 \text{ kg/m}^3$);
- Three different magnetic suspensions, obtained from magnetic clusters functionalized with polyethylene glycol (PEG) and triethylene glycol (TREG) and dispersed in 10 mL distilled water.

The magnetic clusters from the suspensions were targeted using a Neodimium NdFeB52 permanent magnet whose properties are shown in Table 1.

Table 1. Permanent magnet's characteristics used for generating the external magnetic field for the experimental targeting process.

Magnet type	NdFeB52 permanent magnet
Commercial name	N52
Shape	Rectangular
Dimensions (length x width x thickness)	30x20x20 mm
Maximum energy product (BxH)	52 MGOe

Both the magnetic field generated by different types of permanent magnets and the physico-chemical characteristics (size, shape, magnetization and magneto-rheological properties) of the magnetic clusters used in the targeting process are extensively presented in the following chapters of the PhD thesis.

Chapter 3, "Magnetic nanoparticles for drug targeting", discusses theoretical aspects of the different types of magnetic nanoparticles, their properties, synthesis, surface functionalization implications, and in vivo forces acting on the particles in the targeting process. The chapter focuses on iron oxide magnetic nanoparticles (IONPs), which are also the ones used for synthesis and functionalization in this thesis. There are several types of iron oxide nanoparticles, the most studied being magnetite (Fe_3O_4), hematite ($\alpha\text{-Fe}_2\text{O}_3$) and maghemite ($\gamma\text{-Fe}_2\text{O}_3$) [13]. The magnetic properties of these particles depend on their physico-chemical properties, size and shape. Their size also influences how the particles are eliminated from the body following the targeting process. Thus, small particles (< 20 nm) are eliminated via the kidneys, medium-sized particles (30 - 150 nm) via the spinal cord and large particles (150 - 300 nm) via the liver and spleen [14]. In terms of shape, studies show that anisotropic particles (cubes, prisms, etc.) are more difficult to be eliminated from the body than spherical particles [14]. Particles of different shapes and sizes are shown in Figure 4.

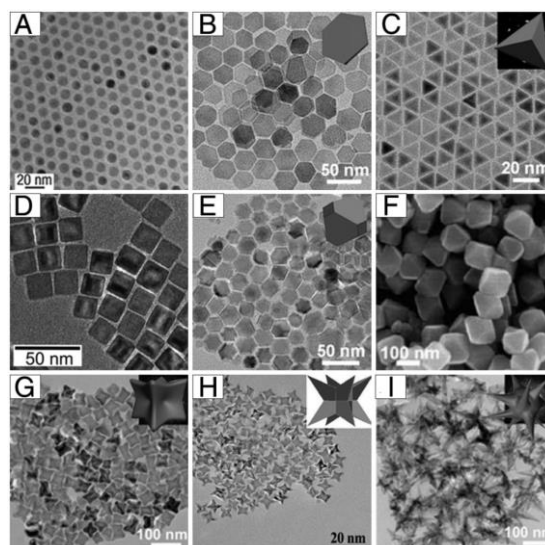


Figure 4. Examples of iron oxide nanoparticles of different shapes and sizes: A) nanospheres, B) plates, C) tetrahedra, D) cubes, E) truncated octahedra, F) octahedra, G) concave, H) octopods, and I) multibranching. Modified according to [15].

There are two primary methods for synthesizing magnetic nanoparticles: top-down or bottom-up. The top-down approach entails breaking down the raw metal material into the nanometric level to create nanoparticles, while the bottom-up method involves the precipitation of Fe_xO_y base molecules, which undergo nucleation and growth until a nanoparticle is formed. Iron oxide nanoparticles can be synthesized using either chemical, physical, or biological methods. Chemical methods are the most commonly used, primarily because they offer low production costs, high yields, and the ability to functionalise the nanoparticles. The most common methods of chemical synthesis for nanoparticles and clusters are co-precipitation, thermal decomposition, sol-gel synthesis, thermal/solvothermal synthesis, microemulsion, sonochemical synthesis and electrochemical synthesis [16]. In the present thesis, the synthesis methods used were thermal decomposition, microemulsion and synthesis by solvothermal method.

Thermal decomposition synthesis consists of the decomposition at high temperatures of organometallic iron precursors in organic solvents. The synthesized iron oxide nanoparticles have improved properties compared to those synthesized by other chemical methods because the nucleation process is separated from the growth process, and complex hydrolysis reactions can be avoided. Due to the high temperatures during the process, thermal decomposition synthesis leads to the formation of IONPs with low polydispersity, narrow size distribution and high crystallinity [17].

Microemulsion synthesis allows the production of nanoparticles in limited quantities within a nano system by combining a stable isotropic mixture of oil and water which is stabilised by a surfactant monolayer. The microemulsion's oil phase contains a hydrophobic structure that is dissolved in the surfactant layer, while the aqueous phase contains a hydrophilic structure. This allows for the presence of metal salts and/or other polar compounds in the aqueous phase, while the organic (oil) phase is made up of various hydrocarbons and olefins. Microemulsion syntheses demonstrated that surfactant type, $\text{Fe}^{2+}/\text{Fe}^{3+}$ ion concentration, droplet size variation, as well as temperature and pH strongly influence nanoparticle formation dynamics, size and magnetization. Despite the narrow size distribution of nanoparticles synthesized through this method, the microemulsion process has certain limitations, such as the difficulty of removing surfactants from the particle surface, large-scale replication of the process or particle aggregation [17].

Solvothermal method synthesis is used to synthesize $\alpha\text{-Fe}_2\text{O}_3$ and Fe_3O_4 particles by crystallization in an organic solvent. The iron precursors are introduced into a hermetically sealed vessel (reactor or autoclave) and exposed to steam under conditions of high temperature ($t = 130 - 250^\circ\text{C}$) and pressure ($p = 0.3 - 4 \text{ MPa}$). This method is used to 'grow' uniform single crystal particles with good control over size and composition and having a higher degree of crystallinity compared to particles synthesized by other means. The solvothermal synthesis method is also useful as to synthesize nanoparticles of specific shapes by changing the concentration of iron precursors [18].

As for the forces acting in vivo on the magnetic particles in the targeting process, they are presented in the following equation, used to calculate the trajectory and velocity of a single particle in a coronary artery:

$$\frac{d}{dt}(m_p \mathbf{v}) = \mathbf{F}_D + \mathbf{F}_L + \mathbf{F}_B + \mathbf{F}_g + \mathbf{F}_m \quad (1)$$

Where: m_p – particle mass, \mathbf{v} – particle velocity, \mathbf{F}_D – hydrodynamic force, \mathbf{F}_L – lift force, \mathbf{F}_B – Brownian force, \mathbf{F}_g – gravitational force, \mathbf{F}_m – magnetophoretic force.

The way in which these forces influence the movement of particles within the blood vessel is shown in Figure 5.

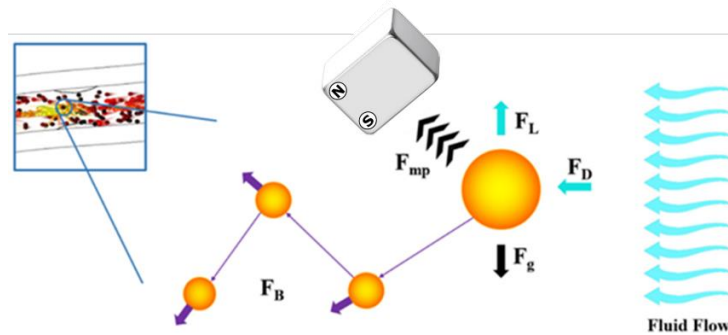


Figure 5. Forces acting on magnetic particles inside the blood vessel. Modified according to [19].

For the present investigations, the Brownian force (F_B) and the gravitational force (F_g) do not interfere, due to particle's small dimensions, and are considered negligible. The lift force (F_L), as it can be seen in Figure 22, acts perpendicular to the flow direction, and was found to be smaller than the hydrodynamic and the magnetophoretic force, being also considered negligible. This leads to only two types of forces influencing the trajectory and velocity of one particle in the artery: the hydrodynamic force (F_D) and the magnetophoretic force (F_{mag}) [20]. These forces are explained in detail within the PhD thesis.

Chapter 4, entitled "Synthesis and characterization of surface functionalized magnetic nanoparticles", follows the chemical process used in the synthesis and functionalization of two types of magnetic particles (spherical and cubic) by thermal decomposition, having the surface coated with polyethylene glycol (PEG). The synthesis of the particles is schematically represented in the following figures:

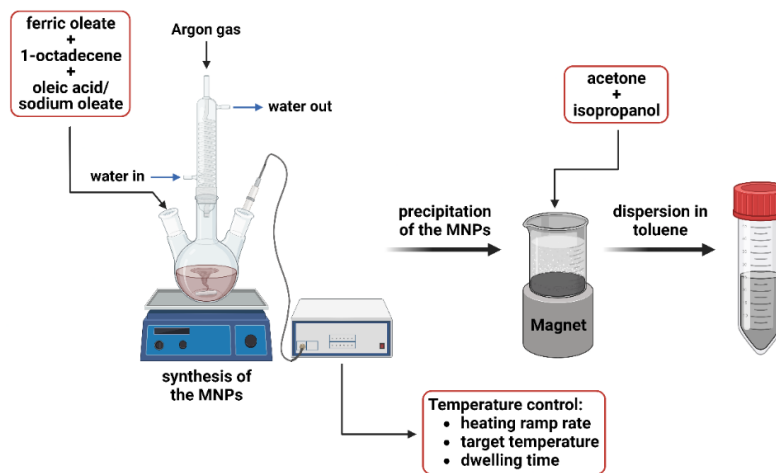


Figure 6. Schematic representation of the synthesis of magnetic nanoparticles by thermal decomposition. Image created with BioRender.com and modified according to [21].

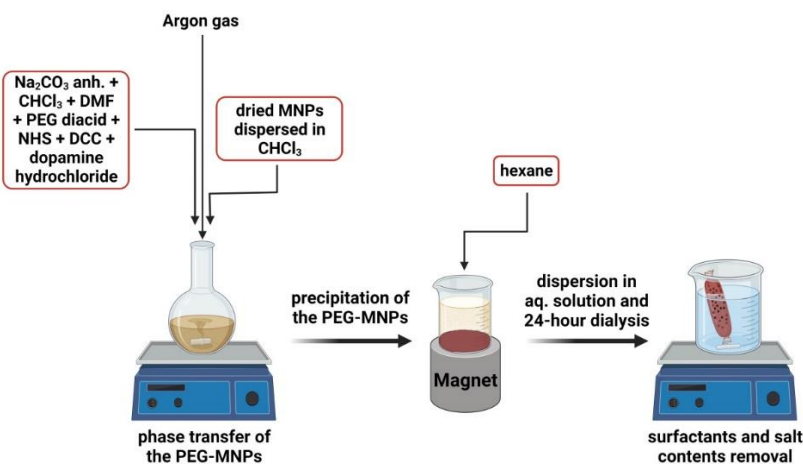


Figure 7. Schematic representation of the phase transfer and PEG coating process of iron oxide nanoparticles. Image created with BioRender.com and modified according to [21].

Following the synthesis, hydrophobic monodisperse magnetic nanoparticles were obtained, with a core size of about 10.2 ± 1.2 nm for the cubic particles and 15.6 ± 1.6 nm for the spherical ones. The core size (D_{TEM}), hydrodynamic diameter (D_H), surfactant layer (D_{OA}), polydispersity (PDI) as well as zeta potential (ZP) are shown in Table 2.

Table 2. Size, polydispersity and zeta potential values associated with the two types of magnetic nanoparticles (spherical and cubic) synthesized through thermal decomposition.

Particles	D_{TEM} [nm]	D_H [nm]	D_{OA} [nm]	PDI	Zeta Potential [mV]
Spherical	10.2 ± 1.2	19.8 ± 0.4	9.8 ± 0.8	0.14	-14
Cubic	15.6 ± 1.6	24.7 ± 5.7	9.2 ± 4.2	0.11	-23.9

These measurements, as well as the presented syntheses, were carried out as part of the PhD internship at the Norwegian University of Science and Technology (NTNU) in Trondheim, Norway, from September to November 2022.

The magnetic particles thus synthesized and characterized had their surface functionalized with polyethylene glycol (PEG). Following their functionalization, agglomerations were formed, with particles' size reaching values between 260 - 300 nm for

cubic and between 300 - 900 nm for spherical particles.

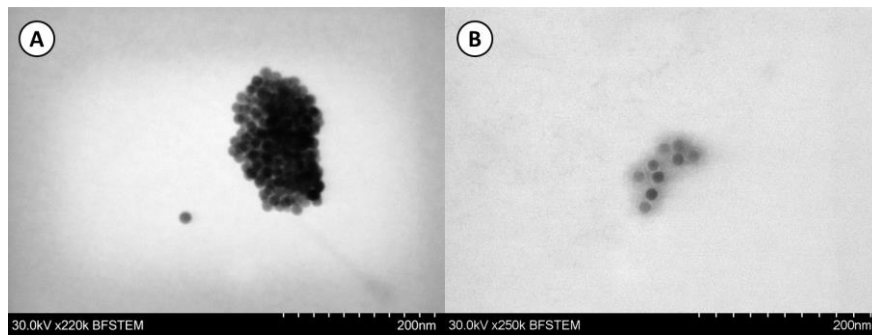


Figure 8. Spherical MNPs after phase transfer reaction and coating of their surface with PEG.

For these functionalized nanoparticles, the hydrodynamic diameter, zeta potential, colloidal stability and response to the action of an external magnetic field, magnetization and magneto-rheological properties for different values of the applied external magnetic field were investigated and measured. These investigations were carried out both during the doctoral internship at the Norwegian University of Science and Technology (NTNU) in Trondheim, Norway, from September to November 2022, and at the Cavitation and Magnetic Liquids Laboratory of the Romanian Academy - Timisoara branch. The aim of the magneto-rheological investigations was to highlight the behavior of the magnetic suspensions both in the presence and absence of an external magnetic field, using a blood analogous fluid (water – glycerol mixture), and its comparison with the magneto-rheological properties of the blood. The magnetic suspensions for both particle types showed higher viscosity compared to blood.

According to the investigations, it was found that an important aspect of the synthesized nanoparticles is that they are hydrophobic due to the surfactant layer on their surface (the surfactant used was oleic acid). Although both types of magnetic nanoparticles exhibited close core dimensions, their magnetization differed significantly. Thus, the magnetization of cubic particles was about twice that of spherical ones. This may be due to the anisotropy of the cubic particles and the surfactant layer influencing the magnetic moment. After the phase transfer reaction and functionalization of the particle surface with polyethylene glycol, the magnetic particles became hydrophilic. A disadvantage of this process is given by the fact that it led to an increase in the size of the hydrodynamic diameter and the formation of agglomerations, especially for spherical particles, which also exhibited poor colloidal stability.

Chapter 5, entitled "Synthesis and characterization of surface-functionalized magnetic clusters", presents the synthesis and characterization of three different types of magnetic clusters using different chemical methods:

1. Magnetic clusters synthesized through thermal decomposition and having the surface functionalized with triethylene glycol (TREG) – **TREG MNC**. This type of clusters were synthesized during the PhD internship carried out at the Norwegian University of Science and Technology (NTNU) in Trondheim, Norway, from November to December 2023.
2. Magnetic clusters synthesized through microemulsion and having the surface functionalized with polyethylene glycol (PEG) – **ME MNC**. These clusters were synthesized by our collaborators at The National Institute for Research and Development of Isotopic and Molecular Technologies (INCDTIM), Cluj-Napoca, Romania.
3. Magnetic clusters synthesized through solvothermal method and having the surface functionalized with polyethylene glycol (PEG) – **ST MNC**. These clusters were synthesized by our collaborators at The National Institute for Research and

Development of Isotopic and Molecular Technologies (INCDTIM), Cluj-Napoca, Romania.

These clusters were characterized in terms of shape, size, magnetization, physico-chemical and magneto-rheological properties. The equivalent surface area and the number of clusters per milliliter of suspension were also calculated for each type of clusters. These measurements are presented in Table 3.

All the investigations were carried out both during the doctoral internship at the Norwegian University of Science and Technology (NTNU) in Trondheim, Norway, from November to December 2023, and at the Cavitation and Magnetic Liquids Laboratory of the Romanian Academy - Timisoara branch.

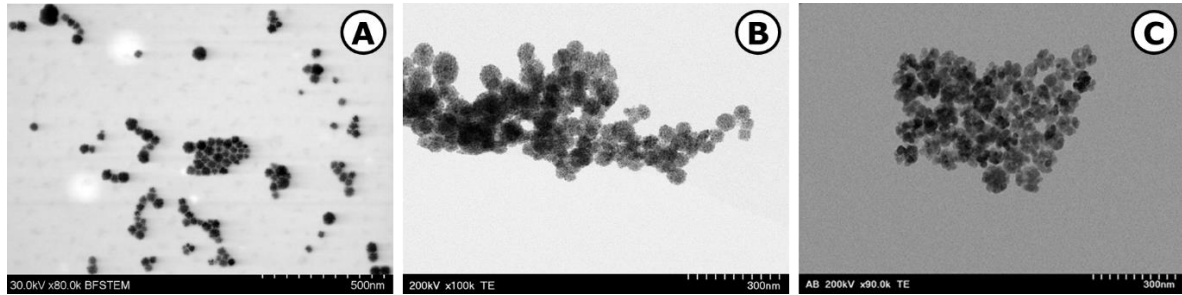


Figure 9. Surface functionalized magnetic clusters synthesized through: (A) thermal decomposition, (B) microemulsion, (C) solvothermal method.

Table 3. Number of magnetic clusters in 1 mL suspension and their equivalent surface for the three types of the investigated clusters.

	TREG MNC	ME MNC	ST MNC
Magnetic clusters number/mL	$20.17 \cdot 10^{12}$	$2.55 \cdot 10^{12}$	$2.02 \cdot 10^{12}$
Equivalent surface [nm²]	$867.48 \cdot 10^{14}$	$243.46 \cdot 10^{14}$	$284.31 \cdot 10^{14}$

Following the investigations, it was observed that each type of clusters has particular characteristics. Thus, in the case of the clusters synthesized through thermal decomposition, they were distinguished by the narrow size distribution and small size diameters (< 100 nm), high zeta potential value, which means that they are stable in suspension, and magnetization with a value of 69.4 emu/g. Their magneto-rheological properties showed that for different values of the applied magnetic field, the difference between the viscosity curves of the clusters is less than one order of magnitude. As for the clusters synthesized through microemulsion and solvothermal method, they exhibited values for the hydrodynamic diameters well above those suitable for medical applications, due to the agglomerations that are formed. The agglomerations may be due to the zeta potential values which suggest their instability in suspension and their tendency to form aggregations over time. By comparing the viscosity curves and magneto-rheological properties for these two types of clusters, it was found that a suspension with 1% clusters synthesized through solvothermal method exhibits the closest behaviour to that of the blood for a shear rate range of $10^{-1} - 10^1$ s⁻¹.

In terms of medical applications, among the three types of clusters, TREG MNC, ME MNC and ST MNC, the magnetic clusters synthesized through thermal decomposition presented the greatest potential due to their small size, good stability and large equivalent surface area that would allow the attachment of a larger amount of medication. All three types of clusters discussed in Chapter 5 were used for experimental targeting investigations using a straight and a stented artery model.

Chapter 6, "Investigation and analysis of the magnetic field generated by permanent magnets", consists of two parts: a theoretical part and a measurement part. The theoretical part provides information on the use of the magnetic field in medical applications, types of permanent magnets and their characteristics, together with their associated advantages and disadvantages, and permanent magnet assemblies. The measurement part investigates numerically and experimentally the magnetic field generated by different combinations of Neodimium-type permanent magnets. A total of 9 types of Neodymium permanent magnets were investigated, having different sizes and grades (grade N35 and N52), noted M1 – M9. For the numerical analysis of the magnetic field, the open-source program FEMM (Finite Element Method Magnetics) was used. Prior to the numerical analysis, a test was performed to discuss the influence of the size of the discretization elements on the magnetic field values. As a result of this test and in order to simplify the numerical calculation for the generation of the magnetic fields of the investigated magnets, the chosen size for the discretization elements was 0.4 mm. The use of FEMM program allowed to observe the magnetic field streamlines (Figure 10), the magnetic flux density and the magnetic field intensity generated by the 9 types of permanent magnets.

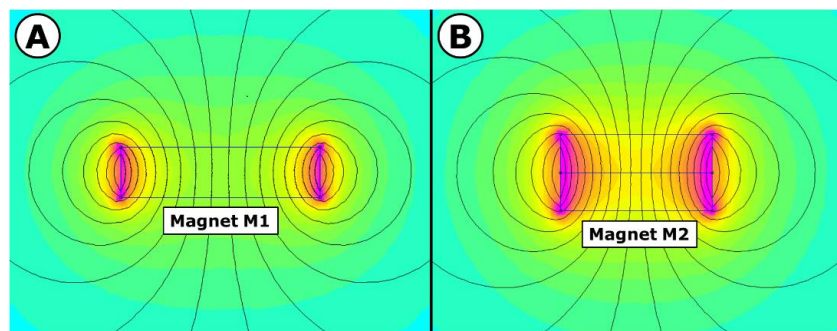


Figure 10. Magnetic field streamlines for magnets M1 (A) and M2 (B) generated in the domain of analysis in the investigation plane.

The numerical values obtained for the magnetic field generated by the permanent magnets were compared with those measured experimentally using a F. W. Bell model 5080 teslameter and a Hall probe. The measurements were performed along all three axes, X, Y and Z, meaning the length and width of the magnet and to a height of 4 cm. The measuring instrument and the associated axes for the measurements are shown in Figure 11.

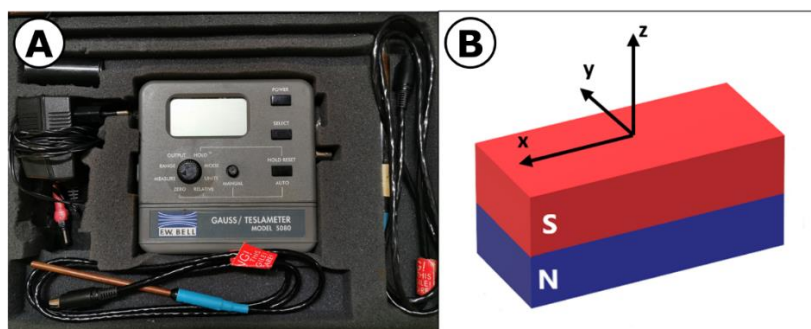


Figure 11. F. W. Bell Model 5080 Teslameter used for magnetic measurements (A). X, Y and Z measurement axes associated to the investigated magnets (B).

The measurements allowed identifying the magnet combinations that generate the strongest magnetic field at a given distance and classified them according to this distance, as shown in Table 4.

Table 4. Classification of magnet combinations according to the distance at which they generate the strongest magnetic field.

Magnets	Distance from magnet surface [mm]	Magnetic field induction [T]
M9	0 – 5	0.597 – 0.376
M5	5 – 30	0.374 – 0.051
M8	35 – 40	0.04 – 0.033

As a result of the measurements and the comparisons that were carried out, the appropriate type of permanent magnet was chosen to be used for the experimental targeting investigations in the thesis.

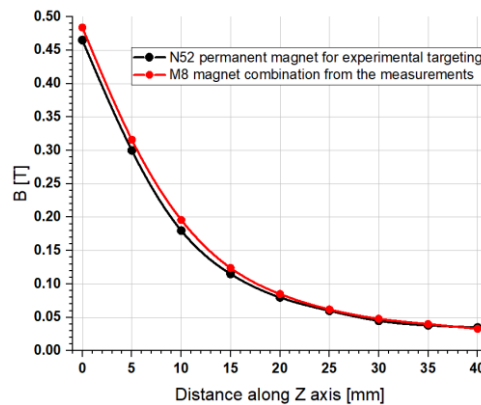


Figure 12. Comparison between the B-field strength evolution along the Z axis for the N52 permanent magnet used for the experimental investigations and the investigated M8 magnet combination.

In Chapter 7, entitled "Numerical simulation of two-phase flow in specific geometries for drug targeting applications", the ANSYS program is used to create simplified 2D and 3D geometries, starting from a 3D stent geometry, in order to use them as to investigate the hemodynamic parameters associated with the fluid flow. For the 2D simplified geometries, two geometries were generated in the Design Modeler extension of ANSYS, one with circular and the other with rectangular struts (Figures 13 and 14). The aim was to quantify the impact of strut geometry on the evolution of fluid flow around the stent struts and the distribution of medication particles in the stented arterial segment.

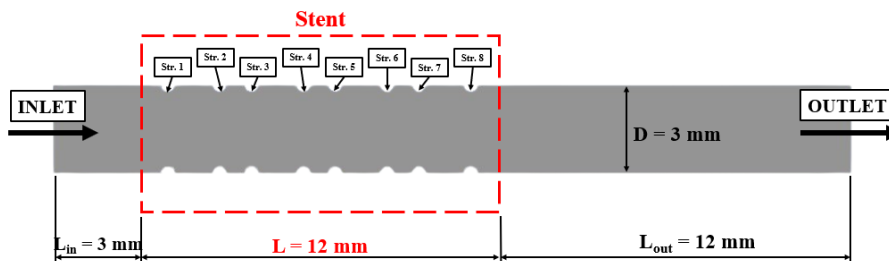


Figure 13. 2D geometry of the circular-type stent placed inside a rigid artery.

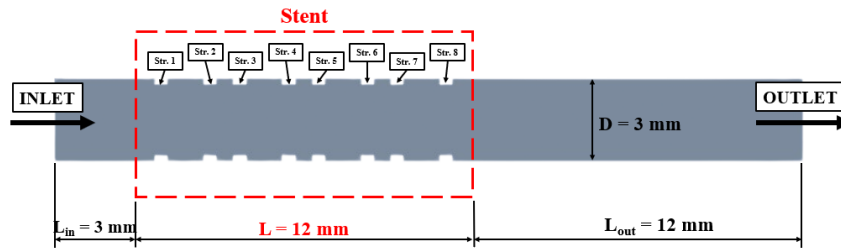


Figure 14. 2D geometry of the square-type stent placed inside a rigid artery.

For the simplified 3D stent geometry, the flow was analysed over a single strut, which is generated as a 3D step (figure 15). The strut's geometry is the 3D equivalent of the 2D square-type strut geometry, i.e. it has the same length and height, but compared to the 2D geometry, it has also thickness. Thus, the strut can be explained as a square rotated around the axis of the artery.

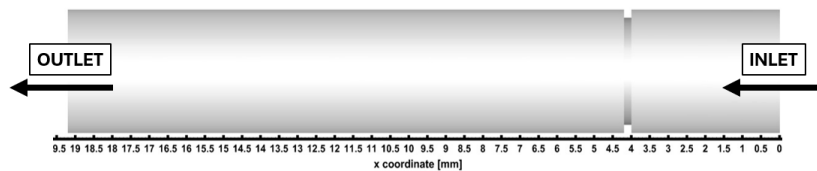


Figure 15. Simplified 3D stent geometry for the numerical analysis with the associated length and inlet and outlet sections.

The flow regime used in the numerical simulations for all types of geometries was pulsatile, with a velocity profile associated with a patient-specific cardiac cycle as a condition for the inlet section. The cardiac cycle time steps used for the numerical investigations were: T1 – beginning of the cardiac cycle, T2 – maximum of the systole, T3 – maximum of the diastole, T4 – mean value on the downward slope of diastole, and T5 – end of the cardiac cycle.

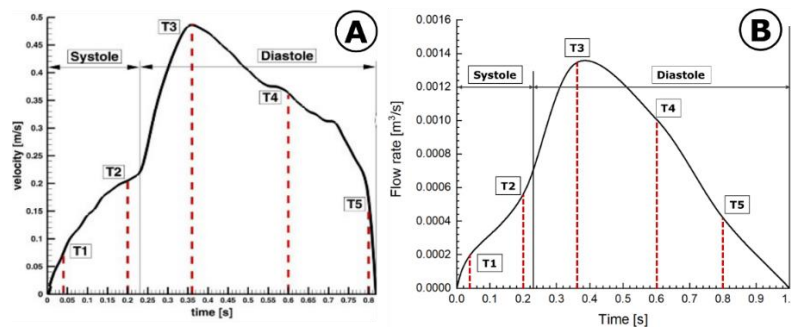


Figure 16. Patient-specific cardiac cycle and the corresponding time steps used for the numerical investigations (A). Cardiac flow rate of the patient-specific cardiac cycle (B).

The hemodynamic parameters and aspects discussed within this chapter were:

- the wall shear stress (WSS) in the vicinity of the stent struts;
- the velocity field;
- the length of recirculation areas;
- the drug release phenomena from struts' surface.

The numerical data indicates that the insertion of a stent into the artery affects the blood flow patterns, particularly in the region adjacent to the arterial wall. In the case of the two simplified stent geometries, these alterations are also a result of the specific strut geometry. In both cases (circular- and square-type strut), regions with low and high values for wall shear

stress were observed. The low WSS values correspond to the vicinity of the struts, where recirculation and stagnation areas are formed. Low WSS values are associated with in stent restenosis while high WSS values may lead to the formation of plaques.

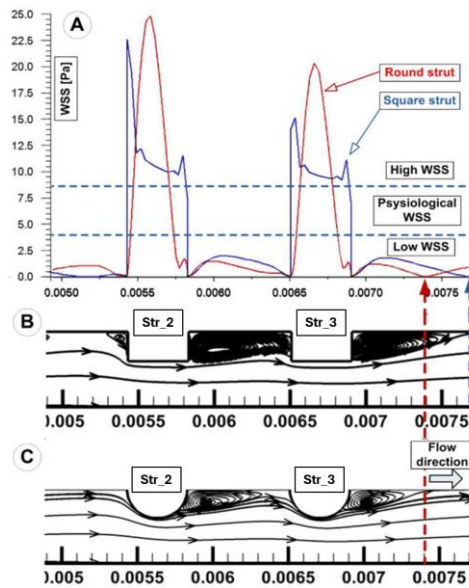


Figure 17. Correlation between the WSS distribution (A) and formation of the recirculation regions for the rectangular (B) and circular (C) strut geometry.

The presence of recirculation regions can prolong the near-wall residence time of drug particles, increasing their concentration and having as negative effect vascular toxicity. The numerical results showed that in the case of a circular-type strut geometry, the recirculation regions are smaller, and the reattachment point to the main flow occurs faster than in the square-type strut geometry. However, from a medical point of view, the square-type strut geometry exhibits better behaviour as the drug particles remain on the strut surface for a longer period. This is important for prolonging the particles' time in the injured area of the blood vessel.

In the case of the 3D simplified stent geometry, the drug release phenomenon showed that the drug particles attached to the left side of the strut remain longer on the surface during a full cardiac cycle. However, when investigating the drug release over three complete cardiac cycle runs, it occurred that most of the drug particles that were attached to strut's surface have been washed away or trapped in flow stagnation zones.

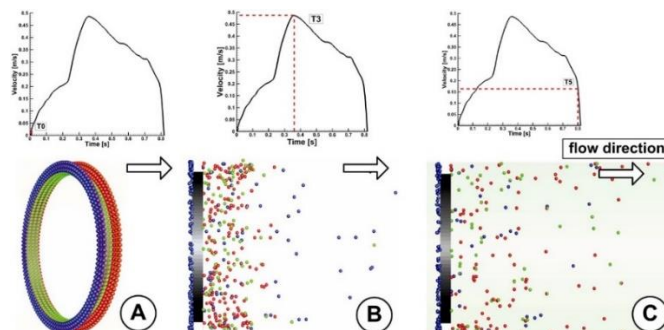


Figure 18. Drug particle distribution by colour around the 3D stent strut at three-time steps of the cardiac cycle: (A) at the beginning of the cardiac cycle, when all drug particles are on the surface of the strut; (B) at the peak of the diastolic phase; and (C) at the end of the cardiac cycle.

Nevertheless, these investigations have been performed on simplified 2D and 3D geometries. When investigating a complex 3D geometry, the obtained results may differ significantly.

Chapter 8, "Experimental investigation of the controlled targeting and deposition of magnetic particles in a straight artery model" aims to investigate the behaviour and comparison of two magnetic suspensions - one with magnetic clusters synthesized through thermal decomposition and TREG on their surface and the other one with magnetic clusters synthesized through solvothermal method and PEG on their surface - in an experimental stand with a straight artery model. The flow regime inside the artery model was pulsatile. The magnetic suspensions was injected into the artery at a constant flow rate. In order to target and capture the magnetic clusters, the permanent magnet chosen and presented in Chapter 6 was placed at a distance of 8, 11, and 14 mm from the lower wall of the arterial model. The different distances between the magnet and the arterial wall correlate with the properties of the magnetic clusters for which the targeting was performed.

The magnetic clusters synthesized through solvothermal method, being larger in size, allowed us to investigate the influence of the distance between the magnet and the arterial wall on particle deposition.

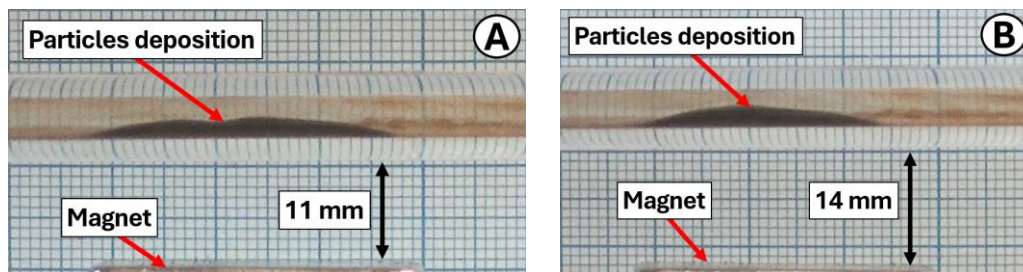


Figure 19. Influence of the distance between the magnet and the arterial model wall on the deposition of the magnetic particles: (A) 11 mm, (B) 14 mm.

When the magnet is positioned closer to the artery wall, the particle accumulation is wider and thinner due to the magnetic field that is stronger and attracts more particles also on the edges of the accumulation. On the other hand, when the magnet is positioned further from the artery, magnetic field's intensity decreases and the particle accumulation is smaller and thicker, with the thickest point in the middle of the accumulation. This point is in accordance with the centre of the magnet, where the magnetic field is the strongest. As a result, by shortening the distance between the magnet and the targeted region of the artery model, the magnetic particle capture efficiency was increased.

Moreover, the accumulation layer has a different pattern both in the case of the ST MNCs and TREG MNCs. Even if for the ST MNCs the molecular weight and the hydrodynamic diameter were bigger, the accumulation thickness of the clusters after $t = 60$ s was the same for both cluster types. The only difference was due to the distance between the artery model and the external magnet, which was of 11 mm ($B = 0.16$ T) for the ST MNCs and 8 mm ($B = 0.22$ T) for the TREG MNCs – because of their smaller dimensions.

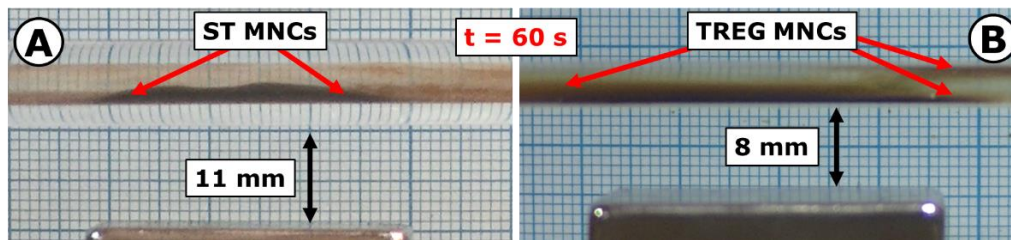


Figure 20. Comparison between the accumulation layer for ST MNCs (A) and TREG MNCs (B) in the straight artery model.

In the case of the ST MNCs, the clusters are strongly deposited on the lower part of the artery model, having a specific geometry. In contrast, the small hydrodynamic sizes of the TREG MNCs leads to a different deposition, where the injected clusters are harder captured by the external magnetic field, as it can be seen in Figure 20B. For the TREG MNCs, a longer period of time is required as for the deposition to stabilize.

Chapter 9, "Experimental investigation of the controlled targeting and deposition of magnetic particles in a stented artery model", similar to Chapter 8, deals with the experimental targeting process of a magnetic suspension containing microemulsion-synthesized magnetic clusters (ME MNCs), with the difference that in the present case a stented artery model is used. Thus, a ferromagnetic stent is introduced in the model of the right artery used for the investigations in Chapter 8, which is the one shown in Figure 21. A ferromagnetic stent can be defined as a stent that could exhibit magnetization, meaning that it would behave like a magnet and attract magnetic clusters.

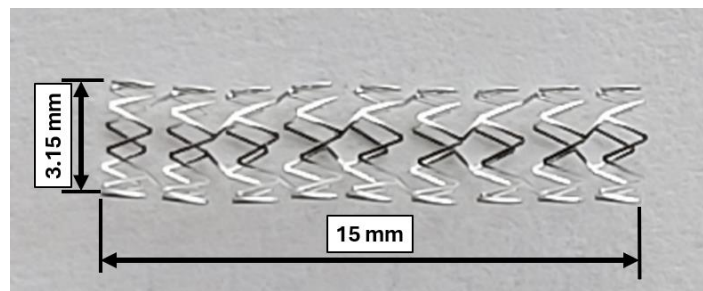


Figure 21. General view of the ferromagnetic stent used for the experimental magnetic targeting investigation and its associated dimensions.

In contrast to the investigations performed in a straight artery model, in the stented artery model the flow was steady-state, the magnetic suspension injection being also performed at a constant flow rate. The deposition of magnetic clusters on the stent surface was followed for a period of 30 seconds.

The use of a stent within an artery results in alterations to the arterial geometry, as well as modifications to the patterns of blood flow and Wall Shear Stress. These changes are responsible for the formation of the recirculation regions in the stented artery area. As to highlight the formation of these regions, before injecting the magnetic suspension, a mixture of glycerol and contrast agent has been introduced into the test section. Figure 22 shows the recirculation regions that are formed in the vicinity of stent's struts. These regions are responsible for trapping drug particles inside for a long period of time, having as consequence areas with increased drug concentration.

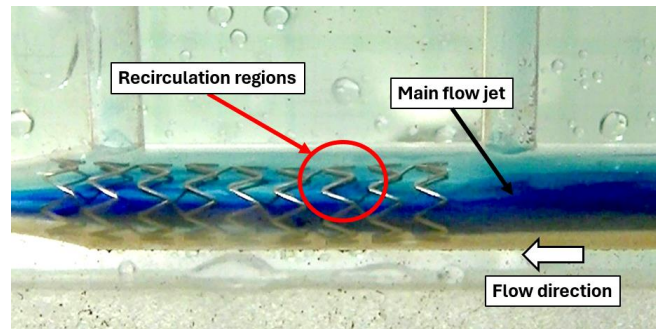


Figure 22. Fluid flow evolution in the stented artery model using a mixture of glycerol and contrast agent. The figure highlights the formation of the recirculation regions. Modified according to [22].

Following the injection, the magnetic clusters progressively cover in time struts' surface and get deposited in the lower area of the stent, especially in the inlet part. The ferromagnetic nature of the stent leads to these clusters getting deposited also on the top of the stent. Thus, magnetically speaking, there is a slightly uniform accumulation of clusters in the stented region.

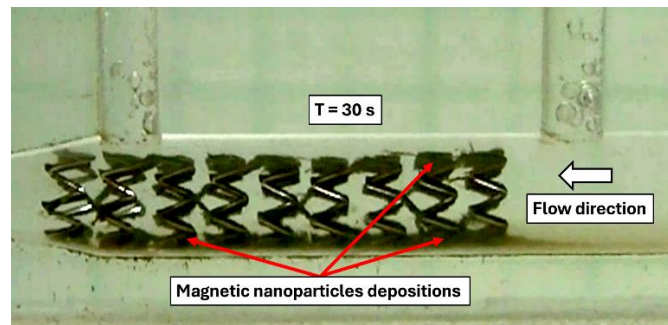


Figure 23. Magnetic particles deposition in the stented artery model for the time step $t = 30$ s. Modified according to [22].

During the experimental investigations, out of the total amount of magnetic clusters from the magnetic suspension which have been injected into the stented artery, a great quantity has been washed away by the flow stream outside the stented segment. This is due to the washing effect and the drag force from the flow stream being stronger compared to the magnetic force and the velocity magnitude inside the artery. In addition to the inlet and outlet sections, the deposition of particles is generally uniformly distributed throughout the stent struts, which is largely influenced by the stent's inherent characteristics, geometry, and the strength of the applied external magnetic field. Even if the ME MNCs present a moderate magnetization (55 emu/g), the clusters manage to cover the stent almost completely and in a thin layer (Figure 109D), as it would be required for medical applications, with only a few struts from the inlet and outlet part of the stent remaining exposed.

Chapter 10 is the chapter of **General Conclusions of the PhD thesis**, structured in four distinct parts: 1. Synthesis and characterization of magnetic particles and clusters, 2. Investigation of the magnetic field generated by permanent magnets, 3. Numerical simulation of the fluid flow in specific 2D and 3D simplified geometries and 4. Experimental targeting of magnetic suspensions in a straight and stented artery model. The findings of this PhD thesis suggest that employing magnetic clusters for the local drug targeting process could be a promising strategy for overcoming the primary disadvantages of systemic drug administration. All the investigated magnetic particles and clusters present advantages and disadvantages in regard to their characteristics and as discussed earlier. As for the clusters used for the experimental targeting in a straight and stented artery model, the ME MNCs offered the best

results, due to the highly coverage of the stent structure, the negative ZP value and the lower viscosity compared to the other analysed magnetic clusters. However, more investigations should be performed as for improving the properties of the potential drug carriers, as well as conducting biocompatibility and toxicity tests. To add more, since the magnetic drug targeting process is a complex technique, its effectiveness relies also on variables such as the strength of the external magnetic field, the geometry of the stent, the arrangement of the stent struts, the stability of the drug and the rate of drug release. These aspects need to be taken into consideration for future research.

The last chapter of the PhD thesis, **Chapter 11**, presents the **personal contributions and perspectives of the author**, which includes among others the synthesis of two types of magnetic nanoparticles and one type of magnetic clusters and their characterization using different instruments (TEM, DLS, XRD, XRD, VSM, FT-IR, TGA). These activities were carried out during the two PhD internships at the Norwegian University of Science and Technology (NTNU) in Trondheim, Norway, at the Particle Engineering Centre from September - November 2022 and November - December 2023.

Regarding author's perspectives, the following research directions can be distinguished:

- Identification, synthesis and characterization of new magnetic particles or clusters with possible biomedical applications. This would involve also the use of surface functionalization with different biopolymers such as chitosan or polyethyleneimine (PEI);
- Improving the synthesis methodology for the solvothermal magnetic clusters as to reduce their size and thus widening the range of their medical applications;
- Investigating the impact of different stent geometries and struts on particle's deposition and fluid flow behaviour;
- Performing numerical simulations on more complex stent geometries as for a clearer perspective over the complex phenomena occurring in the near-wall region of the artery;

The obtained results from the present PhD thesis represent a solid starting point for the formulation of a post-doctoral research topic or a scientific research project for future national project competitions.

References

1. Ahmad, M.; Minhas, M.U.; Sohail, M.; Faisal, M. Comprehensive Review on Magnetic Drug Delivery Systems: A Novel Approach for Drug Targeting. *Journal of Pharmacy and Alternative Medicine* **2013**, *2*, 13–21.
2. Grillone, A.; Ciofani, G. Magnetic Nanotransducers in Biomedicine. *Chemistry A European J* **2017**, *23*, 16109–16114, doi:10.1002/chem.201703660.
3. Iafisco, M.; Alogna, A.; Miragoli, M.; Catalucci, D. Cardiovascular Nanomedicine: The Route Ahead. *Nanomedicine* **2019**, *14*, 2391–2394, doi:10.2217/nnm-2019-0228.
4. Cicha, I.; Alexiou, C. Cardiovascular Applications of Magnetic Particles. *Journal of Magnetism and Magnetic Materials* **2021**, *518*, 167428, doi:10.1016/j.jmmm.2020.167428.
5. Chapman, S.N.; Mehndiratta, P.; Johansen, M.C.; McMurry, T.L.; Johnston, K.C.; Southerland, A.M. Current Perspectives on the Use of Intravenous Recombinant Tissue Plasminogen Activator (tPA) for Treatment of Acute Ischemic Stroke. *Vasc Health Risk Manag* **2014**, *10*, 75–87, doi:10.2147/VHRM.S39213.
6. Ma, Y.-H.; Wu, S.-Y.; Wu, T.; Chang, Y.-J.; Hua, M.-Y.; Chen, J.-P. Magnetically Targeted Thrombolysis with Recombinant Tissue Plasminogen Activator Bound to Polyacrylic Acid-Coated Nanoparticles. *Biomaterials* **2009**, *30*, 3343–3351, doi:10.1016/j.biomaterials.2009.02.034.
7. Chang, M.; Lin, Y.-H.; Gabayno, J.L.; Li, Q.; Liu, X. Thrombolysis Based on Magnetically-Controlled Surface-Functionalized Fe₃O₄ Nanoparticle. *Bioengineered* **2017**, *8*, 29–35, doi:10.1080/21655979.2016.1227145.
8. Prilepskii, A.Y.; Fakhardo, A.F.; Drozdov, A.S.; Vinogradov, V.V.; Dudanov, I.P.; Shtil, A.A.; Bel'tyukov, P.P.; Shibeko, A.M.; Koltsova, E.M.; Nechipurenko, D.Y.; et al. Urokinase-Conjugated Magnetite Nanoparticles as a Promising Drug Delivery System for Targeted Thrombolysis: Synthesis and Preclinical Evaluation. *ACS Appl. Mater. Interfaces* **2018**, *10*, 36764–36775, doi:10.1021/acsami.8b14790.
9. Zhang, Y.; Li, W.; Ou, L.; Wang, W.; Delyagina, E.; Lux, C.; Sorg, H.; Riehemann, K.; Steinhoff, G.; Ma, N. Targeted Delivery of Human VEGF Gene via Complexes of Magnetic Nanoparticle-Adenoviral Vectors Enhanced Cardiac Regeneration. *PLOS ONE* **2012**, *7*, e39490, doi:10.1371/journal.pone.0039490.
10. Arteriosclerosis / Atherosclerosis - Symptoms and Causes Available online: <https://www.mayoclinic.org/diseases-conditions/arteriosclerosis-atherosclerosis/symptoms-causes/syc-20350569> (accessed on 22 June 2022).
11. Valentim, M.X.G.; Zinani, F.S.F.; da Fonseca, C.E.; Wermuth, D.P. Systematic Review on the Application of Computational Fluid Dynamics as a Tool for the Design of Coronary Artery Stents. *Beni-Suef University Journal of Basic and Applied Sciences* **2023**, *12*, 49, doi:10.1186/s43088-023-00382-9.
12. Materón, E.M.; Miyazaki, C.M.; Carr, O.; Joshi, N.; Picciani, P.H.S.; Dalmaschio, C.J.; Davis, F.; Shimizu, F.M. Magnetic Nanoparticles in Biomedical Applications: A Review. *Applied Surface Science Advances* **2021**, *6*, 100163, doi:10.1016/j.apsadv.2021.100163.
13. Vallabani, N.V.S.; Singh, S. Recent Advances and Future Prospects of Iron Oxide Nanoparticles in Biomedicine and Diagnostics. *3 Biotech* **2018**, *8*, 279, doi:10.1007/s13205-018-1286-z.
14. Veiseh, O.; Gunn, J.W.; Zhang, M. Design and Fabrication of Magnetic Nanoparticles for Targeted Drug Delivery and Imaging. *Advanced Drug Delivery Reviews* **2010**, *62*, 284–304, doi:10.1016/j.addr.2009.11.002.
15. Xie, W.; Guo, Z.; Gao, F.; Gao, Q.; Wang, D.; Liaw, B.; Cai, Q.; Sun, X.; Wang, X.; Zhao, L. Shape-, Size- and Structure-Controlled Synthesis and Biocompatibility of Iron Oxide

- Nanoparticles for Magnetic Theranostics. *Theranostics* **2018**, *8*, 3284–3307, doi:10.7150/thno.25220.
16. Ali, A.; Zafar, H.; Zia, M.; Haq, I. ul; Phull, A.R.; Ali, J.S.; Hussain, A. Synthesis, Characterization, Applications, and Challenges of Iron Oxide Nanoparticles. *NSA* **2016**, *9*, 49–67, doi:10.2147/NSA.S99986.
 17. Wu, W.; Wu, Z.; Yu, T.; Jiang, C.; Kim, W.-S. Recent Progress on Magnetic Iron Oxide Nanoparticles: Synthesis, Surface Functional Strategies and Biomedical Applications. *Science and Technology of Advanced Materials* **2015**, *16*, 023501, doi:10.1088/1468-6996/16/2/023501.
 18. Chen, Y.; Zhang, J.; Wang, Z.; Zhou, Z. Solvothermal Synthesis of Size-Controlled Monodispersed Superparamagnetic Iron Oxide Nanoparticles. *Applied Sciences* **2019**, *9*, 5157, doi:10.3390/app9235157.
 19. Forouzandehmehr, M.; Ghoytasi, I.; Shamloo, A.; Ghosi, S. Particles in Coronary Circulation: A Review on Modelling for Drug Carrier Design. *Materials & Design* **2022**, *216*, 110511, doi:10.1016/j.matdes.2022.110511.
 20. Mahmoodpour, M.; Goharkhah, M.; Ashjaee, M. Investigation on Trajectories and Capture of Magnetic Drug Carrier Nanoparticles after Injection into a Direct Vessel. *Journal of Magnetism and Magnetic Materials* **2020**, *497*, 166065, doi:10.1016/j.jmmm.2019.166065.
 21. Ioncica, M.-C.; Bandyopadhyay, S.; Bali, N.; Socoliuc, V.; Bernad, S.I. Investigation of Cubic and Spherical IONPs' Rheological Characteristics and Aggregation Patterns from the Perspective of Magnetic Targeting. *Magnetochemistry* **2023**, *9*, 99, doi:10.3390/magnetochemistry9040099.
 22. Bernad, S.I.; Craciunescu, I.; Sandhu, G.S.; Dragomir-Daescu, D.; Tombacz, E.; Vekas, L.; Turcu, R. Fluid Targeted Delivery of Functionalized Magnetoresponse Nanocomposite Particles to a Ferromagnetic Stent. *Journal of Magnetism and Magnetic Materials* **2021**, *519*, 167489, doi:10.1016/j.jmmm.2020.167489.